Solar and Atmospheric Four–Neutrino Oscillations

M. C. Gonzalez-Garcia[1,2] *, M. Maltoni[2] †, C. Peña-Garay[1,2] ‡

[1] *Theory Division, CERN CH1221, Geneva 23, Switzerland*

[2]*Instituto de Física Corpuscular, Universitat de València – C.S.I.C*

Edificio Institutos de Paterna, Apt 22085, 46071 València, Spain

Abstract

We present an analysis of the neutrino oscillation solutions of the solar and atmospheric neutrino problems in the framework of four–neutrino mixing where a sterile neutrino is added to the three standard ones and the mass spectra presents two separated doublets. Such scenarios allow for simultaneous transitions of solar ν_e, as well as atmospheric ν_μ, into active and sterile neutrinos controlled by the additional mixing angles ϑ_{23} and ϑ_{24}, and they contain as limiting cases the pure solar ν_e–active and ν_e–sterile neutrino oscillations, and the pure atmospheric $\nu_\mu \to \nu_s$ and $\nu_\mu \to \nu_\tau$ oscillations, respectively. We evaluate the allowed active–sterile admixture in both solar and atmospheric oscillations from the combined analysis. Our results show that, although the Super–Kamiokande data disfavour both the pure $\nu_\mu \to \nu_s$ atmospheric channel and the pure $\nu_e \to \nu_s$ solar channel, the result from the combined analysis still favours close–to–pure active and sterile oscillations and disfavours oscillations into a near–maximal active–sterile admixture.

*concha@thwgs.cern.ch

†maltoni@ific.uv.es

‡penya@ific.uv.es

I. INTRODUCTION

Super–Kamiokande high statistics data [1–3] indicate that the observed deficit in the μ-like atmospheric events is due to the neutrinos arriving at the detector at large zenith angles, strongly suggestive of the ν_μ oscillation hypothesis. Similarly, their data on the zenith angle dependence and recoil energy spectrum of solar neutrinos [4,5] in combination with the results from Homestake [8], SAGE [9], and GALLEX+GNO [10,11] experiments, have put on a firm observational basis the long–standing problem of solar neutrinos, strongly indicating the need for ν_e conversions.

In addition to the solar and atmospheric neutrino results from underground experiments, there is also the indication for neutrino oscillations in the $\bar{\nu}_\mu \rightarrow \bar{\nu}_e$ channel by the LSND experiment [12]. All these results can be accommodated in a single oscillation framework only if there are at least three different scales of neutrino mass-squared differences. The simplest case in which this condition is satisfied requires the existence of a fourth light neutrino, which must be *sterile* (*i.e.* having interactions with standard model particles much weaker than the SM weak interaction) in order not to affect the invisible Z decay width, precisely measured at LEP [13–17].

There are various analyses in the literature comparing the oscillation channels into active or sterile neutrinos for both solar [21–23] and atmospheric data [18,19] performed in the framework of two–neutrino oscillations (where oscillations occur into either an active or a sterile state). In particular the Super–Kamiokande collaboration has claimed the oscillation into sterile neutrinos to be disfavoured both for solar [6] and atmospheric neutrinos [7]. However, when considered in the framework of four–neutrino mixing, oscillations into pure active or pure sterile states are only limiting cases of the most general possibility of oscillations into an admixture of active and sterile neutrinos [17]. Such a more general framework of four–neutrino mixing has also been analysed in recent studies, which have put constraints on the active–sterile admixture either in the context of solar [24] or atmospheric [25–27] neutrino oscillations, respectively.

In this paper we present a *combined* analysis of the neutrino oscillation solutions of both the solar and the atmospheric neutrino problem, in the framework of four–neutrino mixing. We include in our analysis the most recent solar neutrino rates of Homestake [8], SAGE [9], GALLEX and GNO [10,11], as well as the recent 1258 day Super–Kamiokande data sample [5], including the recoil electron energy spectrum for both day and night periods. As for atmospheric neutrinos we include in our analysis all the contained event from the latest 79.5 kton-yr Super–Kamiokande data set [3], as well as the upward-going neutrino-induced muon fluxes from both Super–Kamiokande and the MACRO detector [28]. The constraints arising from relevant reactor (mainly from Bugey [29]) and accelerator (CDHSW [30] and CCFR [31]) experiments are also imposed.

The outline of the paper is the following. In Sec. II we summarize the main expressions for the neutrino oscillation formulas that we use in the analysis of solar and atmospheric neutrino data which take into account matter effects both in the propagation in the Sun and in the Earth. Sections III and IV contain the results for the analysis of the four–neutrino oscillation parameters for solar and atmospheric data respectively. The results for the full combined analysis are described in Sec. V, with particular emphasis on the active–sterile oscillation admixture which better allows for a simultaneous description of the solar and

atmospheric neutrino data. Our results show that, against what may be naively expected, although the Super–Kamiokande data disfavours both the pure $\nu_\mu \rightarrow \nu_s$ atmospheric channel and the pure $\nu_e \rightarrow \nu_s$ solar channel, the result from the combined analysis still favours any of these close–to–pure active and sterile oscillations and disfavours oscillations into a near–maximal active–sterile admixture.

II. FOUR–NEUTRINO OSCILLATIONS

There are six possible four–neutrino schemes that can accommodate the results from solar and atmospheric neutrino experiments as well as the LSND evidence. They can be divided in two classes: $3+1$ and $2+2$. In the $3+1$ schemes there is a group of three neutrino masses separated from an isolated one by a gap of the order of 1 eV^2 which is responsible for the short-baseline oscillations observed in the LSND experiment. In $2+2$ schemes there are two pairs of close masses separated by the LSND gap. $3+1$ schemes are disfavoured by experimental data with respect to the $2+2$ schemes [15,16], but they are still marginally allowed [32]. Therefore we concentrate in the $2+2$ schemes shown in Fig. 1. For the phenomenology of neutrino oscillations these two schemes are equivalent up to the relabeling of the mass eigenstates (or equivalently of the mixing angles). Thus in what follows we will consider the scheme B where the mass spectrum presents the hierarchy:

$$\Delta m^2_\odot = \Delta m^2_{21} \ll \Delta m^2_{\text{atm}} = \Delta m^2_{43} \ll \Delta m^2_{\text{LSND}} = \Delta m^2_{41} \simeq \Delta m^2_{42} \simeq \Delta m^2_{31} \simeq \Delta m^2_{32} \quad (2.1)$$

(we use the common notation $\Delta m^2_{kj} \equiv m^2_k - m^2_j$). In this four-neutrino mixing scheme, the flavour neutrino fields ν_α ($\alpha = e, s, \mu, \tau$) are related to the mass eigenstates fields ν_k by

$$\nu_\alpha = \sum_{k=1}^{4} U_{\alpha k}\, \nu_k \qquad (\alpha = e, s, \mu, \tau) \,, \tag{2.2}$$

where U is a 4×4 unitary mixing matrix. Neglecting possible CP phases, the matrix U can be written as a product of six rotations, U_{12}, U_{13}, U_{14}, U_{23}, U_{24} and U_{34} where

$$(U_{ij})_{ab} = \delta_{ab} + (c_{ij} - 1)\,(\delta_{ia}\delta_{ib} + \delta_{ja}\delta_{jb}) + s_{ij}\,(\delta_{ia}\delta_{jb} - \delta_{ja}\delta_{ib}) \,. \tag{2.3}$$

where $c_{ij} = \cos \vartheta_{ij}$ and $s_{ij} = \sin \vartheta_{ij}$. The order of the product of the matrices corresponds to a specific parametrization of the mixing matrix U. In order to study oscillations of the solar and atmospheric neutrinos which include the matter effects in the Sun and/or in the Earth, it is convenient to use the following parametrization [17]:

$$U = U_{24}\, U_{23}\, U_{14}\, U_{13}\, U_{34}\, U_{12} \,. \tag{2.4}$$

This general form can be further simplified by taking into account the negative results from the reactor experiments, in particular the Bugey one [29] which implies that

$$P^{Bugey}_{ee} = 1 - 2\left(|U_{e1}|^2 + |U_{e2}|^2\right)\left(1 - |U_{e1}|^2 - |U_{e2}|^2\right)\langle\sin^2\frac{\Delta m^2_{\text{LSND}}L}{4E}\rangle \gtrsim 0.99 \tag{2.5}$$

in the range of Δm^2_{41} relevant for the LSND experiment. This leads to an upper bound on the projection of the ν_e over the 3–4 states:

$$|U_{e3}|^2 + |U_{e4}|^2 = c_{14}^2 s_{13}^2 + s_{14}^2 \lesssim 10^{-2} \tag{2.6}$$

so that the two angles ϑ_{13} and ϑ_{14} must be small and their contribution to solar and atmospheric neutrino transitions is negligible. Therefore, in what follows we will set these two angles to zero, although one must keep in mind that at least one of them must be non-vanishing in order to account for the LSND observation.

In the approximation $\vartheta_{13} = \vartheta_{14} = 0$ the U matrix takes the form:

$$U = \begin{pmatrix} c_{12} & s_{12} & 0 & 0 \\ -s_{12}c_{23}c_{24} & c_{12}c_{23}c_{24} & s_{23}c_{24}c_{34} - s_{24}s_{34} & s_{23}c_{24}s_{34} + s_{24}c_{34} \\ s_{12}s_{23} & -c_{12}s_{23} & c_{23}c_{34} & c_{23}s_{34} \\ s_{12}c_{23}s_{24} & -c_{12}c_{23}s_{24} & -s_{23}s_{24}c_{34} - c_{24}s_{34} & -s_{23}s_{24}s_{34} + c_{24}c_{34} \end{pmatrix}. \tag{2.7}$$

In the rest of this section we will discuss the consequences of the mixing structure of Eq. (2.7) on the relevant transition probabilities for solar and atmospheric neutrino oscillations. The transition probabilities that take into account matter effects have been derived in Ref. [17]. Some improvement concerning the calculation of the regeneration of solar ν_e's in the Earth was presented in Ref. [24]. Here we summarize the discussion on the flavour composition of the relevant states for both solar and atmospheric neutrino oscillations.

A. Solar Neutrinos

In the scheme here considered, solar neutrino oscillations are generated by the mass-squared difference between ν_2 and ν_1. It is clear from Eq. (2.7) that the survival of solar ν_e's mainly depends on the mixing angle ϑ_{12}, whereas the mixing angles ϑ_{23} and ϑ_{24} determine the relative amount of transitions into sterile ν_s or active ν_μ and ν_τ. Let us remind the reader that ν_μ and ν_τ cannot be distinguished in solar neutrino experiments, since their matter potential and their interaction in the detectors are due only to neutral-current weak interactions and therefore they are equal. Thus, instead of ν_μ and ν_τ, one can consider the linear combinations

$$\begin{pmatrix} \nu_a \\ \nu_b \end{pmatrix} = \begin{pmatrix} \cos\vartheta & \sin\vartheta \\ -\sin\vartheta & \cos\vartheta \end{pmatrix} \begin{pmatrix} \nu_\mu \\ \nu_\tau \end{pmatrix}, \tag{2.8}$$

with

$$\cos\vartheta = -\frac{s_{23}}{\sqrt{1 - c_{23}^2 c_{24}^2}}, \qquad \sin\vartheta = -\frac{s_{24}c_{23}}{\sqrt{1 - c_{23}^2 c_{24}^2}}. \tag{2.9}$$

The mixing of ν_a and ν_b with ν_1 and ν_2 is given by

$$U_{a1} = -s_{12}\sqrt{1 - c_{23}^2 c_{24}^2}, \quad U_{a2} = c_{12}\sqrt{1 - c_{23}^2 c_{24}^2}, \quad U_{b1} = U_{b2} = 0, \tag{2.10}$$

so that the solar neutrino oscillations occur only between the states

$$\nu_e \rightarrow \nu_\alpha \quad \text{with} \quad \nu_\alpha = c_{23}c_{24}\nu_s + \sqrt{1 - c_{23}^2 c_{24}^2}\,\nu_a, \tag{2.11}$$

with mixing angle ϑ_{12}, and

3

$$c_{23}^2 c_{24}^2 = 1 - |U_{a1}|^2 - |U_{a2}|^2 = |U_{s1}|^2 + |U_{s2}|^2 , \tag{2.12}$$

gives the size of the projection of the sterile neutrino onto the state in which the solar ν_e oscillates to.

Therefore, solar neutrino oscillations depend only on ϑ_{12} and the product $c_{23}c_{24}$. We distinguish the following limiting cases of Eq. (2.11):

- if $c_{23}c_{24} = 0$ then $U_{s1} = U_{s2} = 0$, $U_{a1} = -s_{12}$, $U_{a2} = c_{12}$, corresponding to the limit of pure two-generation $\nu_e \to \nu_a$ transitions;

- if $c_{23}c_{24} = 1$ then $U_{s1} = s_{12}$, $U_{s2} = c_{12}$ and $U_{a1} = U_{a2} = 0$ and we have the limit of pure two-generation $\nu_e \to \nu_s$ transitions.

Since the mixing of ν_e with ν_1 and ν_2 is described by a two-generation equation with mixing angle ϑ_{12}, the mixing of ν_s with ν_1 and ν_2 is given by the same formula multiplied by $c_{23}c_{24}$, and the mixing of ν_a with ν_1 and ν_2 is again described by the same equation times $\sqrt{1 - c_{23}^2 c_{24}^2}$, it is clear that, in the general case of simultaneous $\nu_e \to \nu_s$ and $\nu_e \to \nu_a$ oscillations, the corresponding probabilities are given by

$$P_{\nu_e \to \nu_s}^{\text{Sun+Earth}} = c_{23}^2 c_{24}^2 \left(1 - P_{\nu_e \to \nu_e}^{\text{Sun+Earth}} \right) , \tag{2.13}$$

$$P_{\nu_e \to \nu_a}^{\text{Sun+Earth}} = \left(1 - c_{23}^2 c_{24}^2 \right) \left(1 - P_{\nu_e \to \nu_e}^{\text{Sun+Earth}} \right) . \tag{2.14}$$

where $P_{\nu_e \to \nu_e}^{Sun+Earth}$ takes the standard two–neutrino oscillation form [23] for Δm_{21}^2 and ϑ_{12}, found by numerically solving the evolution equation in the Sun and the Earth matter with the modified matter potential

$$A \equiv A_{CC} + c_{23}^2 c_{24}^2 A_{NC} . \tag{2.15}$$

with $A_{CC} = 2\sqrt{2}G_F E N_e$ and $A_{NC} = -\sqrt{2}G_F E N_n$. Here N_e and N_n are, respectively, the number densities of electrons and neutrons in the medium, E is the neutrino energy and G_F is the Fermi constant. These expressions satisfy the relation of probability conservation $P_{\nu_e \to \nu_e}^{\text{Sun+Earth}} + P_{\nu_e \to \nu_s}^{\text{Sun+Earth}} + P_{\nu_e \to \nu_a}^{\text{Sun+Earth}} = 1$.

The analysis of the solar neutrino data in the four–neutrino mixing schemes is therefore equivalent to the two–neutrino analysis but taking into account that the parameter space is now three–dimensional $(\Delta m_{21}^2, \tan^2 \vartheta_{12}, c_{23}^2 c_{24}^2)$. Although originally this derivation was performed in the framework of the $2 + 2$ schemes [17,24], it is equally valid for the $3 + 1$ ones [33].

Let us finally comment on the range of variation of the mixing parameters. Choosing the convention that $\Delta m_{21}^2 \geq 0$, from Eqs. (2.13) and (2.14) it is clear that for solar neutrino oscillations the full physical space is covered by choosing the mixing angles in the ranges:

$$0 \leq \vartheta_{12} \leq \frac{\pi}{2} , \qquad 0 \leq \vartheta_{23} \leq \frac{\pi}{2} , \qquad 0 \leq \vartheta_{24} \leq \frac{\pi}{2} . \tag{2.16}$$

Actually, since the dependence on ϑ_{23} and ϑ_{24} enters only through the combination $c_{23}^2 c_{24}^2$, for what concerns the solar neutrino phenomenology one of these mixing angles could be fixed to zero. However, as we will see in the next section, they enter independently in the relevant probabilities for atmospheric neutrinos.

4

B. Atmospheric Neutrinos

Atmospheric neutrino oscillations are generated by the mass-squared difference between ν_3 and ν_4. From Eq. (2.7) one sees that the atmospheric ν_e's are not affected by the four–neutrino oscillations in the approximation $\vartheta_{13} = \vartheta_{14} = 0$ and neglecting the effect of Δm_{21}^2 in the range of atmospheric neutrino energies. Conversely the survival probability of atmospheric ν_μ's mainly depends on the mixing angle ϑ_{34}. The mixing angles ϑ_{23} and ϑ_{24} determine the relative amount of ν_μ transitions into sterile ν_s or active ν_τ. More explicitly Eq. (2.7) implies that the atmospheric neutrino oscillations, *i.e.* oscillations with the mass difference Δm_{34}^2 and mixing angle ϑ_{34}, occur between the states

$$\nu_\beta \to \nu_\gamma \quad \text{with} \quad \nu_\beta = s_{23}c_{24}\nu_s + c_{23}\nu_\mu - s_{23}s_{34}\nu_\tau \quad \text{and} \quad \nu_\gamma = s_{24}\nu_s + c_{24}\nu_\tau . \tag{2.17}$$

We distinguish the following limiting cases of Eq. (2.17):

- if $c_{23} = 1$ then $U_{\mu 1} = U_{\mu 2} = 0$. The atmospheric $\nu_\mu = \nu_\beta$ state oscillates into a state $\nu_\gamma = c_{24}\nu_\tau + s_{24}\nu_s$. This is the limit studied in Ref. [25,26]. We will denote this case as "restricted". In particular:

    - in the case $c_{23} = c_{24} = 1$ we have $U_{s3} = U_{s4} = 0$, corresponding to the limit of pure two–generation $\nu_\mu \to \nu_\tau$ transitions;
    - in the case $c_{23} = 1$ and $c_{24} = 0$ we have $U_{\tau 3} = U_{\tau 4} = 0$, corresponding to the limit of pure two–generation $\nu_\mu \to \nu_s$ transitions;

- if $c_{23} = 0$ there are not atmospheric neutrino oscillations as the projection of ν_μ over the relevant states cancels out ($U_{\mu 3} = U_{\mu 4} = 0$).

Thus the mixing angle ϑ_{23} determines the size of the projection of the ν_μ over the "atmospheric" neutrino oscillating states,

$$s_{23}^2 = |U_{\mu 1}|^2 + |U_{\mu 2}|^2 = 1 - |U_{\mu 3}|^2 - |U_{\mu 4}|^2. \tag{2.18}$$

As a consequence, one expects s_{23} to be small in order to explain the atmospheric neutrino deficit and, as we will see in Sec. IV, this is the case. Furthermore, the negative results from the CDHS [30] and CCFR [31] experiments on searches for ν_μ–disappearance also constrain such projection to be

$$s_{23}^2 = |U_{\mu 1}|^2 + |U_{\mu 2}|^2 \lesssim 0.2 \tag{2.19}$$

at 90% CL for $\Delta m_{\text{LSND}}^2 \gtrsim 0.4 \text{ eV}^2$.

Approximate expressions for the relevant ν_μ survival probability including matter effects in the Earth can be found in Ref. [17]. For what concerns the work presented here, the relevant probabilities can be calculated by numerically integrating the evolution equation in the Earth with the modified matter potential

$$A \equiv (s_{24}^2 - s_{23}^2 c_{24}^2) A_{NC} , \tag{2.20}$$

so that for pure atmospheric $\nu_\mu \to \nu_\tau$ oscillations ($s_{23}^2 = s_{24}^2 = 0$) $A = 0$, while for $\nu_\mu \to \nu_s$ ($s_{23}^2 = 0$, $s_{24}^2 = 1$) $A = A_{NC}$, as expected. It is this modification of the Earth matter

potential what gives to the atmospheric neutrino data the capability to discriminate between the active and sterile oscillation solution. In particular, higher sensitivity to this potential effect is achievable for the higher energy part of the atmospheric neutrino flux which lead to the upward going muon data. The main effect of the presence of this potential is that for pure active oscillations the angular distribution of upgoing muons is expected to be steeper at larger arrival angles, while a flattening is expected due to the matter effects for sterile oscillations [20].

From Eqs. (2.17) and (2.20) we see that, unlike in the case of solar neutrinos, the angles ϑ_{23} and ϑ_{24} enter independently in the atmospheric oscillations. Thus the analysis of the atmospheric neutrino data in the four–neutrino mixing schemes is equivalent to the two–neutrino analysis but taking into account that the parameter space is now four–dimensional $(\Delta m_{43}^2, \vartheta_{34}, c_{23}^2, c_{24}^2)$.

Concerning the range of variation of the mixing angles, the full parameter space relevant for atmospheric neutrino oscillation can be covered by choosing ϑ_{23} and ϑ_{24} in the ranges indicated in Eq. (2.16), but, in general, the mixing angle ϑ_{34} must be allowed to take values in the interval

$$-\frac{\pi}{2} \leq \vartheta_{34} \leq \frac{\pi}{2} \tag{2.21}$$

(in the convention $\Delta m_{43}^2 \geq 0$). In the limiting case $\vartheta_{23} = 0$, there is an additional symmetry in the relevant probabilities so that the full parameter space can be spanned by $0 \leq \vartheta_{34} \leq \frac{\pi}{2}$, as expected since in this case we have the effective two–neutrino oscillation $\nu_\mu \to \nu_\gamma$.

III. SOLAR NEUTRINO ANALYSIS

We first describe the results of the analysis of the solar neutrino data in terms of ν_e oscillations. We determine the allowed range of oscillation parameters using the total event rates of the Chlorine [8], Gallium [9–11] and Super–Kamiokande [5] (corresponding to the 1258 days data sample) experiments. For the Gallium experiments we have used the weighted average of the results from GALLEX+GNO and SAGE detectors. We have also included the Super–Kamiokande electron recoil energy spectrum measured separately during the day and night periods. This will be referred in the following as the day–night spectra data which contains $19 + 19$ data bins. The analysis includes the latest standard solar model fluxes, BP00 model [34], with updated distributions for neutrino production points and solar matter density.

For details on the statistical analysis applied to the different observables we refer to Ref. [21,23]. As discussed in the previous section, the analysis of the solar neutrino data in these four–neutrino mixing schemes is equivalent to the two–neutrino analysis but taking into account that the parameter space is now three–dimensional $(\Delta m_{21}^2, \tan^2 \vartheta_{12}, c_{23}^2 c_{24}^2)$, so we have a total of 37 degrees of freedom (d.o.f.).

We first present the results of the allowed regions in the three–parameter space for the global combination of solar observables. Notice that since the parameter space is three–dimensional the allowed regions for a given CL are defined as the set of points satisfying the condition

$$\chi_{\text{sol}}^2(\Delta m_{12}^2, \vartheta_{12}, c_{23}^2 c_{24}^2) - \chi_{\text{sol,min}}^2 \leq \Delta\chi^2(\text{CL, 3 d.o.f.}) \tag{3.1}$$

where, for instance, $\Delta\chi^2(\text{CL, 3 d.o.f.}) = 6.25, 7.81$, and 11.34 for CL $= 90\%, 95\%$ and 99% respectively, and $\chi^2_{\text{sol,min}}$ is the global minimum in the three–dimensional space.

In Fig. 2 we plot the sections of such a volume in the plane $(\Delta m^2_{21}, \tan^2(\vartheta_{12}))$ for different values of the active–sterile admixture $|U_{s1}|^2 + |U_{s2}|^2 = c^2_{23}c^2_{24}$. The global minimum used in the construction of the regions lies in the LMA region and for pure ν_e–active oscillations

$$|U_{s1}|^2 + |U_{s2}|^2 = c^2_{23}c^2_{24} = 0$$
$$\Delta m^2_{21} = 3.65 \times 10^{-5} \text{ eV}^2$$
$$\tan^2 \vartheta_{21} = 0.37$$
$$\chi^2_{\text{sol,min}} = 37.1 \tag{3.2}$$

which for 37 d.o.f. (3 rates $+$ 38 spectrum points $-$ 1 spectrum free normalization $-$ 3 parameters) corresponds to a goodness of the fit (GOF) of 46%.

As seen in Fig. 2 the SMA region is always a valid solution for any value of $c^2_{23}c^2_{24}$ at 99% CL. This is expected as in the two–neutrino oscillation picture this solution holds both for pure ν_e–active and pure ν_e–sterile oscillations. Notice, however, that the statistical analysis is different: in the two–neutrino picture the pure ν_e–active and ν_e–sterile cases are analysed separately, whereas in the four–neutrino picture they are taken into account simultaneously in a consistent scheme. On the other hand, both the LMA and LOW solutions disappear for larger values of the active–sterile admixture.

Let us comment here that, unlike for the case of atmospheric neutrinos where the discrimination between active and sterile oscillations arises from the difference in the matter potentials, for solar neutrinos the main source of difference is due to the lack of neutral current contribution to the water Cerenkov experiments for the sterile case. Unlike active neutrinos which lead to events in the Super–Kamiokande detector by interacting via NC with the electrons, sterile neutrinos do not contribute to the Super–Kamiokande event rates. Therefore a larger survival probability for ^{8}B neutrinos is needed to accommodate the measured rate. As a consequence a larger contribution from ^{8}B neutrinos to the Chlorine and Gallium experiments is expected, so that the small measured rate in Chlorine can only be accommodated if no ^{7}Be neutrinos are present in the flux. This is only possible in the SMA solution region, since in the LMA and LOW regions the suppression of ^{7}Be neutrinos is not enough. Notice also that the SMA region for oscillations into sterile neutrinos is slightly shifted downwards as compared to the active case. This is due to the small modification of the neutrino survival probability induced by the different matter potentials. The matter potential for sterile neutrinos is smaller than for active neutrinos due to the negative NC contribution proportional to the neutron abundance. For this reason the resonant condition for sterile neutrinos is achieved at lower Δm^2.

In Fig. 3 we plot the difference $\Delta\chi^2_{\text{sol}}$ between the local minimum of χ^2_{sol} for each solution and the global minimum in the three–dimensional space, as a function of the active–sterile admixture $|U_{s1}|^2 + |U_{s2}|^2 = c^2_{23}c^2_{24}$. From the figure we find that:

- solar neutrino data favours pure $\nu_e \to \nu_a$ oscillations but sizable active–sterile admixtures are allowed;

- the dependence of $\Delta\chi^2_{\text{sol}}$ on the active-sterile admixture is very gentle in the SMA region while it is much more pronounced for the LMA solution;

- the three dimensional regions disappear at 90% (99%) CL for the following value of $c_{23}^2 c_{24}^2$

$$|U_{s1}|^2 + |U_{s2}|^2 = c_{23}^2 c_{24}^2 < 0.08 \ (1.) \qquad \text{for SMA,}$$
$$|U_{s1}|^2 + |U_{s2}|^2 = c_{23}^2 c_{24}^2 < 0.43 \ (0.71) \quad \text{for LMA,} \qquad (3.3)$$
$$|U_{s1}|^2 + |U_{s2}|^2 = c_{23}^2 c_{24}^2 < 0.3 \ (0.77) \quad \text{for LOW-QVO;}$$

- at 95% CL the three–dimensional LMA region is allowed for maximal active–sterile mixing $c_{23}^2 c_{24}^2 = 0.5$ while at 99% CL all solutions are possible for maximal admixture.

There is a subtlety on the meaning of these limiting values of the mixing $c_{23}^2 c_{24}^2$. The values quoted in Eq. (3.3) correspond to the mixings at which the corresponding three–dimensional region disappears at a given CL. Strictly speaking this is not the same as the allowed range of $c_{23}^2 c_{24}^2$ at a given CL when the parameters $(\tan^2 \vartheta_{12}, \Delta m_{21}^2)$ are left free to vary, either in the full parameter space or within a given solution. Such limits would be obtained by imposing the condition $\Delta \chi_{\text{sol}}^2 = \chi_{\text{sol,min 12}}^2(c_{23}^2 c_{24}^2) - \chi_{\text{sol,min}}^2 \leq \Delta \chi^2(\text{CL, 1 d.o.f.})$ where $\chi_{\text{sol,min 12}}^2(c_{23}^2 c_{24}^2)$ is minimized in the parameter space 1–2 (or in a given region of such parameter space) and $\chi_{\text{sol,min}}^2$ is minimized in the same region of the space 1–2 and in the mixing $c_{23}^2 c_{24}^2$.

In what follows we label as "constrained" the results of analyses when the parameters Δm_{21}^2 and ϑ_{12} are varied within a given solution while "unconstrained" refers to the case where we allow the variation of Δm_{21}^2 and ϑ_{12} in the full plane. For the unconstrained fit the corresponding curve in Fig. 3 is simply the lower envolvent of the curves from the constrained analysis, and it follows the LMA curve for $0 \leq c_{23}^2 c_{24}^2 \leq 0.46$ and the SMA one for $0.46 \leq c_{23}^2 c_{24}^2 \leq 1$.

IV. ATMOSPHERIC NEUTRINO ANALYSIS

In our statistical analysis of the atmospheric neutrino events we use all the samples of Super–Kamiokande data: e-like and μ-like data samples of sub- and multi-GeV [3], each given as a 5-bin zenith-angle distribution*, and upgoing muon data including the stopping (5 bins in zenith-angle) and through–going (10 angular bins) muon fluxes. We have also included the latest MACRO [28] upgoing muon samples, with 10 angular bins which is also sensitive to the active–sterile admixture. So we have a total 45 independent inputs.

For details on the statistical analysis applied to the different observables we refer to Ref. [18,35]. As discussed in the previous section the analysis of the atmospheric neutrino data in these four–neutrino mixing schemes is equivalent to the two–neutrino analysis but taking into account that the parameter space is now four–dimensional $(\Delta m_{43}^2, \vartheta_{34}, c_{23}^2, c_{24}^2)$. Alternatively we present the results in the equivalent parameter space $(\Delta m_{43}^2, \vartheta_{34}, |U_{\mu1}|^2 + |U_{\mu2}|^2, |U_{s1}|^2 + |U_{s2}|^2)$.

We first present the results of the allowed regions in the four–parameter space for the global combination of atmospheric observables. Notice that since the parameter space is

---

*Note that for convenience and maximal statistical significance we prefer to bin the Super–Kamiokande contained event data in 5, instead of 10 bins.

4–dimensional the allowed regions for a given CL are defined as the set of points satisfying the condition

$$\chi^2_{\text{atm}}(\Delta m^2_{43}, \vartheta_{34}, c^2_{23}, c^2_{24}) - \chi^2_{\text{atm,min}} \leq \Delta\chi^2(\text{CL, 4 d.o.f.}) \tag{4.1}$$

where $\Delta\chi^2(\text{CL, 4 d.o.f.}) = 7.78$, 9.49, and 13.3 for CL = 90%, 95% and 99% respectively, and $\chi^2_{\text{atm,min}}$ is the global minimum in the four–dimensional space.

In Fig. 4 we plot the sections of such a volume in the plane $(\Delta m^2_{43}, \sin^2(\vartheta_{34}))$ for different values of the mixings ϑ_{23} and ϑ_{24}, which we parametrize by values of the projections $|U_{\mu1}|^2 + |U_{\mu2}|^2$ and $|U_{s1}|^2 + |U_{s2}|^2$. As discussed in Sec. II for arbitrary values of c^2_{23} and c^2_{24} the full parameter space is covered for ϑ_{34} in the range given in Eq. (2.21). In Fig. 4 we display this full parameter space by showing the region in $(\Delta m^2_{43}, \text{sgn}(\vartheta_{34})\sin^2(\vartheta_{34}))$ with "positive" $\sin^2(\vartheta_{34})$ for $0 < \vartheta_{34} \leq \frac{\pi}{2}$ and "negative" $\sin^2(\vartheta_{34})$ for $-\frac{\pi}{2} \leq \vartheta_{34} < 0$. As seen from the figure the parameter space is composed of two separated regions, each of them around maximal mixing $\vartheta_{34} = \pm\frac{\pi}{4}$.

The global minimum used in the construction of the regions lies almost in the pure atmospheric ν_μ–ν_τ oscillations. At the best fit point:

$$
\begin{aligned}
|U_{s1}|^2 + |U_{s2}|^2 &= c^2_{23}c^2_{24} = 0.97 \\
|U_{\mu1}|^2 + |U_{\mu2}|^2 &= s^2_{23} = 0.01 \\
\Delta m^2_{43} &= 2.4 \times 10^{-3} \text{ eV}^2 \\
\vartheta_{34} &= 39° \\
\chi^2_{\text{atm,min}} &= 29.0
\end{aligned}
\tag{4.2}
$$

which for $45 - 4 = 41$ d.o.f. corresponds to a GOF of 92%. A careful reader may find this GOF surprisingly high. Let us comment here that there has been a reduction of the χ^2 with respect to previous analysis [18,35] due to a better agreement of the 79.5 SK electron distribution with the non-oscillation expectation (same effect is found in Ref. [26]). Since the scenarios here discussed do not affect the atmospheric ν_e predictions, this implies an overall improvement on the GOF of any these four–neutrino oscillation schemes.

From Fig. 4 we see that the region becomes considerably smaller for increasing values of the mixing angle ϑ_{23}, which determines the size of the projection of the ν_μ over the "atmospheric" neutrino oscillating states, and for increasing values of the mixing angle ϑ_{24}, which determines the active–sterile admixture in which the "almost–ν_μ" oscillates to. Therefore from the analysis of the atmospheric neutrino data we obtain an upper bound on both mixings which, in particular, implies a lower bound on the combination $c^2_{23}c^2_{24} = |U_{s1}|^2 + |U_{s2}|^2$ limited from above by the solar neutrino data. To quantify these bounds we display in Fig. 6.a the allowed region in the parameter space $(s^2_{23} = |U_{\mu1}|^2 + |U_{\mu2}|^2, c^2_{23}c^2_{24} = |U_{s1}|^2 + |U_{s2}|^2)$. Following the discussion below Eq. (3.3) we obtain the allowed two–dimensional region by imposing the condition

$$\Delta\chi^2_{\text{atm}} = \chi^2_{\text{atm,min 34}}(\vartheta_{23}, \vartheta_{24}) - \chi^2_{\text{min}} \leq \Delta\chi^2(\text{CL, 2 d.o.f.}) \tag{4.3}$$

where $\chi^2_{\text{atm,min 34}}(\vartheta_{23}, \vartheta_{24})$ is minimized with respect to Δm^2_{43} and ϑ_{34} and $\chi^2_{\text{atm,min}}$ is the global minimum in the four–dimensional parameter space. The diagonal cut in Fig. 6.a gives the unitarity bound

$$|U_{\mu 1}|^2 + |U_{\mu 2}|^2 + |U_{s1}|^2 + |U_{s2}|^2 = |U_{\tau 3}|^2 + |U_{\tau 4}|^2 \leq 1 \qquad (4.4)$$

where we have used that in Eq. (2.7) $U_{e3} = U_{e4} = 0$. As seen from Fig. 6.a, the analysis of the atmospheric data imposes a severe bound on the ν_μ projection. For instance, the two–dimensional region extends only till

$$s_{23}^2 = |U_{\mu 1}|^2 + |U_{\mu 2}|^2 \lesssim 0.12 \ (0.16) \qquad (4.5)$$

at 90% (99%) CL, which, as previously mentioned (see Eq. (2.19)), is perfectly consistent with the bounds from the ν_μ–disappearance accelerator experiments CDHDW [30] and CCFR [31] given in Eq. (2.19).

In order to determine the impact of the small but possible deviation from zero of s_{23}^2 we also study the "restricted" case of Ref. [25,26] in which we impose $s_{23}^2 = |U_{\mu 1}|^2 + |U_{\mu 2}|^2 = 0$. In this case the parameter space for atmospheric neutrino oscillation is three–dimensional and the allowed regions for a given CL are defined as the set of points satisfying the condition

$$\chi_{atm}^2(\Delta m_{43}^2, \vartheta_{34}, c_{24}^2) - \chi_{atm,min}^2 \leq \Delta\chi^2(\text{CL, 3 d.o.f.}) . \qquad (4.6)$$

In Fig. 5 we plot the sections of this volume in the plane $(\Delta m_{43}^2, \sin^2(\vartheta_{34}))$ for different values of c_{24}^2. As discussed in Sec. II for the "restricted" case the full parameter space is covered with $0 \leq \vartheta_{34} \leq \frac{\pi}{2}$. This is graphically displayed in Fig. 5, where the symmetry $\vartheta_{34} \to -\vartheta_{34}$ is clearly evident.

The constrains on the active–sterile admixture in the two cases are displayed in Fig. 6.b, where we plot the dependence of $\Delta\chi_{atm}^2$ on the active–sterile admixture $c_{23}^2 c_{24}^2 = |U_{s1}|^2 + |U_{s2}|^2$, both in the general case (i.e. when χ_{atm}^2 is minimized with respect to all other parameters in the problem), and in the "restricted" case (for which the ν_μ projection has been fixed $|U_{\mu 1}|^2 + |U_{\mu 2}|^2 = 0$). The horizontal lines are the values of $\Delta\chi^2(\text{CL, 1 d.o.f.})$ for CL = 90% and 99%. From this figure we obtain the 90% (99%) CL lower bounds on $c_{23}^2 c_{24}^2$ from the analysis of the atmospheric neutrino data:

$$c_{23}^2 c_{24}^2 = |U_{s1}|^2 + |U_{s2}|^2 > 0.64 \ (0.52) \qquad (4.7)$$
$$c_{24}^2 = |U_{s1}|^2 + |U_{s2}|^2 > 0.83 \ (0.74) \quad \text{for the restricted case.} \qquad (4.8)$$

As seen in the figure $\Delta\chi_{atm}^2$ has a monotonically growing behaviour as $|U_{s1}|^2 + |U_{s2}|^2$ decreases for $|U_{s1}|^2 + |U_{s2}|^2 \gtrsim 0.4$–0.6, while the dependence flattens below that value with the presence of a shallow secondary minimum around $|U_{s1}|^2 + |U_{s2}|^2 \sim 0.25$–0.3. We have traced the presence of this secondary minimum to the combined effect of the behaviour of χ^2 for the different sets of upgoing muon data. For all sets of upgoing muon data the best fit is very close to the global minimum in Eq. (4.2). MACRO data at the moment leads to a monotonically growing χ^2 as the sterile admixture grows while Super–Kamiokande upgoing data on both stopping and through-going muons presents a flattening of their χ^2 for $|U_{s1}|^2 + |U_{s2}|^2 \leq 0.5$–0.6. This lost of sensitivity of Super–Kamiokande at larger sterile admixtures arises from the fact that their latest upgoing muon data presents a flattening of the muon suppression in the angular bins for arrival directions around $-0.7 \leq \cos\theta \leq -0.4$ which is compatible with large sterile admixtures. The same effect has been found in Ref. [26]. When combining the χ^2 for Macro and Super–Kamiokande data samples and taking into account the strong correlation

10

between their respective theoretical errors, we find the appearance of this secondary shallow minimum.

From the figure we see that oscillations into a pure sterile state are excluded at 99.97% CL as compared to pure active oscillations. One must notice, however, that taken as an independent scenario, $\nu_\mu \rightarrow \nu_s$ oscillations give a $\chi^2_{min} = 46$ (for $45 - 2$ d.o.f.) which implies a GOF of 35% and therefore cannot be ruled out in the bases of its absolute quality.

In summary, we see that the analysis of the atmospheric data implies that:

- one of the two–neutrino states in the 3–4 oscillating pair must be a close–to–pure ν_μ;

- this close–to–pure ν_μ oscillates into a state which is preferably composed by ν_τ, although a 48% admixture of sterile in this state is still allowed at 99% CL;

- when imposing the "restricted" condition that one of the states is a pure ν_μ, the bound on the sterile admixture is tightened approximately by a factor 2 (from 48% to 26% at 99% CL).

V. COMBINED ANALYSIS: CONCLUSIONS

From the previous sections we have learned that the analysis of the solar data favours the scenario in which the solar oscillations in the plane 1–2 are ν_e oscillations into an active neutrino, and from that analysis we found an upper limit on the projection of the ν_s on the 1–2 states. On the other hand, the atmospheric neutrino analysis prefers that the oscillations of the 3–4 states occur between a close–to–pure ν_μ and an active (ν_τ) neutrino, so giving an upper bound on the projection of the ν_s over the 3–4 states or equivalently a lower bound on its projection over the 1–2 states. The open question is then what is the best scenario for the active–sterile admixture once these two bounds are put together.

To address this question in full generality we have studied the behaviour of the global $\chi^2_{\text{atm+sol}}$ function defined as

$$
\begin{aligned}
\chi^2_{\text{atm+sol}}(\Delta m^2_{21}, \vartheta_{12}, \Delta m^2_{43}, \vartheta_{34}, \vartheta_{23}, \vartheta_{24}) = \\
\chi^2_{\text{sol}}(\Delta m^2_{21}, \vartheta_{23}, c^2_{23}c^2_{24}) + \chi^2_{\text{atm}}(\Delta m^2_{43}, \vartheta_{34}, c^2_{23}, c^2_{24})
\end{aligned}
\tag{5.1}
$$

with the mixing angles ϑ_{23} and ϑ_{24} determining the active–sterile admixture for the following scenarios:

- ATM+SOL$_{\text{unc}}$: in this case we minimize $\chi^2_{\text{atm+sol}}$ with respect to Δm^2_{21}, ϑ_{12}, Δm^2_{43} and ϑ_{34}, allowing Δm^2_{21} and ϑ_{12} to change from LMA to SMA as the active–sterile admixture controlled by ϑ_{23} and ϑ_{24} change. The ν_μ projection $s^2_{23} = |U_{\mu 1}|^2 + |U_{\mu 2}|^2$ is free to vary in the range allowed by the analysis;

- ATM$_{\text{R}}$+SOL$_{\text{unc}}$: in this case we fix $s^2_{23} = |U_{\mu 1}|^2 + |U_{\mu 2}|^2 = 0$, so $|U_{s1}|^2 + |U_{s2}|^2 = c^2_{24}$. We minimize $\chi^2_{\text{atm+sol}}$ with respect to Δm^2_{21}, ϑ_{12}, Δm^2_{43} and ϑ_{34}, allowing Δm^2_{21} and ϑ_{12} to change from LMA to SMA as the mixing angle ϑ_{24} changes;

- ATM+SOL$_{\text{LMA(SMA)}}$: in this case we minimize $\chi^2_{\text{atm+sol}}$ with respect to Δm^2_{21}, ϑ_{12}, Δm^2_{43} and ϑ_{34} with Δm^2_{21} and ϑ_{12} constrained to be in the LMA (SMA) region. The ν_μ projection $s^2_{23} = |U_{\mu 1}|^2 + |U_{\mu 2}|^2$ is free to vary in the range allowed by the analysis;

- ATM$_R$+SOL$_{\rm LMA(SMA)}$: in this case we fix $s_{23}^2 = |U_{\mu 1}|^2 + |U_{\mu 2}|^2 = 0$, so $|U_{s1}|^2 + |U_{s2}|^2 = c_{24}^2$. We minimize $\chi^2_{\rm atm+sol}$ with respect to Δm_{21}^2, ϑ_{12}, Δm_{43}^2 and ϑ_{34}, with Δm_{21}^2 and ϑ_{12} constrained to be in the LMA (SMA) region.

In Table I we give the values $\chi^2_{\rm min,atm+sol}$ of the best fit point and its associated GOF in the six–dimensional (five–dimensional for the "restricted" case) space in each of these cases together with the best fit value of the mixings $|U_{\mu 1}|^2 + |U_{\mu 2}|^2 = s_{23}^2$ and $|U_{s1}|^2 + |U_{s2}|^2 = c_{23}^2 c_{24}^2$. In Fig. 7 we plot the shift in χ^2 from the corresponding global minimum in each of the scenarios as the mixing $|U_{s1}|^2 + |U_{s2}|^2 = c_{23}^2 c_{24}^2$ varies. From the table and the figure we find the following behaviours:

- there are two favourite configurations which we will denote as near–pure–sterile solar neutrino oscillations plus near–pure–active atmospheric neutrino oscillations (NPSS+NPAA), and close–to–active solar neutrino oscillations plus close–to–sterile atmospheric neutrino oscillations (CAS+CSA), respectively. NPSS+NPAA oscillations are characterized by the minima

$$|U_{s1}|^2 + |U_{s2}|^2 \sim 0.91\text{--}0.97 \,, \tag{5.2}$$

  where the exact position of the minimum depends on the allowed admixture $|U_{\mu 1}|^2 + |U_{\mu 2}|^2$. CAS+CSA oscillations are characterized by the minima

$$|U_{s1}|^2 + |U_{s2}|^2 \sim 0.18\text{--}0.2 \,. \tag{5.3}$$

  In both the cases the minima are not very deep in χ^2 (this is particularly the case for CAS+CSA);

- in none of the cases maximal active–sterile (MAS) admixture $|U_{s1}|^2 + |U_{s2}|^2 = c_{23}^2 c_{24}^2 = 0.5$ is favoured.

The scenarios with the solar solution either within the SMA region (Fig. 7.c) or left unconstrained (Fig. 7.a) prefer the NPSS+NPAA scenario. They give a better fit to the combined analysis with a GOF of 66%–68%. In these cases the dependence of $\chi^2_{\rm atm+sol}$ with the active–sterile admixture is more pronounced and it is dominated by the dependence of the atmospheric neutrino analysis, although there is a secondary minimum at the CAS+CSA configuration which for the ATM+SOL$_{\rm unc}$ case is acceptable at 92% CL. In all these scenarios MAS admixture is ruled out at more than 99% CL. Qualitatively this behaviour arises from the fact that in these scenarios increasing the sterile admixture in the atmospheric pair is strongly disfavoured while it is still acceptable for the solar pair since the SMA solution is valid for pure $\nu_e \to \nu_s$ solar oscillations.

On the other hand, the scenarios with the solar solution within the LMA region (Fig. 7.b) prefer the CAS+CSA scenario, although the dependence of $\chi^2_{\rm atm+sol}$ with the active–sterile admixture is not very strong and it presents a secondary minimum near the complementary situation of close–to–sterile solar plus close–to–active atmospheric (CSS+CAA) scenario, which is acceptable at 90% CL. They give the worst fit to the combined analysis but they still present an acceptable GOF: 47.5% (56%) for the "restricted" (unrestricted) case. In these scenarios MAS admixture is ruled out at 99% CL for the "restricted" case and it is

acceptable at about 95% CL for the unrestricted one. This behaviour arises from the fact that in these scenarios increasing the sterile admixture both in the atmospheric pair and in the solar case is strongly disfavoured. It is precisely in this case that one would expect the combined solution to lie near MAS admixture. However, the results show that it is the solar dependence (which dominates in the combination) what leads to the slightly better description for the CAS+CSA scenario with a secondary minimum at the complementary CSS+CAA scenario.

Summarizing, in this paper we have performed a combined analysis of the neutrino oscillation solutions of the solar and atmospheric neutrino problem in the framework of four–neutrino mixing. Such scenarios allow for simultaneous transitions of solar ν_e as well as atmospheric ν_μ into active and sterile neutrinos. Our results show that although the solar and atmospheric data analyzed independently disfavour the pure $\nu_\mu \to \nu_s$ atmospheric channel and the pure $\nu_e \to \nu_s$ solar channel, the result from the combined analysis still favours close–to–pure active and sterile oscillations either in the solar or in the atmospheric sector (depending on the selected solar solution) and disfavours oscillations into a near–maximal active–sterile admixture.

ACKNOWLEDGMENTS

REFERENCES

[1] Y. Fukuda *et al.*, Phys. Lett. **B433**, 9 (1998); Phys. Lett. **B436**, 33 (1998).

[2] Y. Fukuda *et al.*, Phys. Lett. **B467**, 185 (1999); Phys. Rev. Lett. **82**, 2644 (1999).

[3] Super–Kamiokande presentations in winter conferences: C. McGrew in *Neutrino Telescopes 2001*, 9th International Workshop on Neutrino Telescopes (Venice, Italy, March 2001), to appear; T. Toshito in *Moriond 2001*, XXXVI Rencontres de Moriond on Electroweak Interactions and Unified Theories (Les Arcs, France, March 2001), to appear.

[4] Super–Kamiokande Collaboration, Y. Fukuda *et al.*, Phys. Rev. Lett. **81**, 1158 (1998); Erratum **81**, 4279 (1998); **82**, 1810 (1999); **82**, 2430 (1999); Y. Suzuki, Nucl. Phys. B (Proc. Suppl.) **77**, 35 (1999).

[5] S. Fukuda *et al.* [Super–Kamiokande Collaboration], hep-ex/0103032.

[6] S. Fukuda *et al.* [Super–Kamiokande Collaboration], hep-ex/0103033.

[7] S. Fukuda *et al.* [Super–Kamiokande Collaboration], Phys. Rev. Lett. **85**, 3999 (2000).

[8] B. T. Cleveland *et al.*, Astrophys. J. **496**, 505 (1998); R. Davis, Prog. Part. Nucl. Phys. **32**, 13 (1994); K. Lande, talk at XIX International Conference on Neutrino Physics and Astrophysics, Sudbury, Canada, June 2000 (*http://nu2000.sno.laurentian.ca*);

[9] SAGE Collaboration, J. N. Abdurashitov *et al.*, Phys. Rev. **C60**, 055801 (1999); V. Gavrin, talk at XIX International Conference on Neutrino Physics and Astrophysics, Sudbury, Canada, June 2000 (*http://nu2000.sno.laurentian.ca*).

[10] GALLEX Collaboration, W. Hampel *et al.*, Phys. Lett. **B447**, 127 (1999).

[11] E. Belloti, talk at XIX International Conference on Neutrino Physics and Astrophysics, Sudbury, Canada, June 2000 (*http://nu2000.sno.laurentian.ca*).

[12] C. Athanassopoulos, Phys. Rev. Lett. **75** 2650 (1995); Phys. Rev. Lett. **77** 3082 (1996); Phys. Rev. Lett. **81** 1774 (1998).

[13] J.T. Peltoniemi, D. Tommasini and J.W.F. Valle, Phys. Lett.**B298**, 383 (1993); E.J. Chun *et al.*, Phys. Lett.**B357**, 608 (1995); S.C. Gibbons *et al.*, Phys. Lett. **B430**, 296 (1998); B. Brahmachari and R.N. Mohapatra, Phys. Lett. **B437**, 100 (1998); S. Mohanty, D.P. Roy and U. Sarkar, Phys. Lett. **B445**, 185 (1998); J.T. Peltoniemi and J.W.F. Valle, Nucl. Phys. **B406**, 409 (1993); Q.Y. Liu and A.Yu. Smirnov, Nucl. Phys. **B524**, 505 (1998); D.O. Caldwell and R.N. Mohapatra, Phys. Rev. **D48**, 3259 (1993); E. Ma and P. Roy, Phys. Rev. **D52**, R4780 (1995); A.Yu. Smirnov and M. Tanimoto, Phys. Rev. **D55**, 1665 (1997); N. Gaur *et al.*, Phys. Rev. **D58**, 071301 (1998); E.J. Chun, C.W. Kim and U.W. Lee, Phys. Rev. **D58**, 093003 (1998); K. Benakli and A.Yu. Smirnov, Phys. Rev. Lett. **79**, 4314 (1997); Y. Chikira, N. Haba and Y. Mimura, Eur. Phys. J. C **16**, 701 (2000); C. Liu and J. Song, Phys. Rev. **D60**, 036002 (1999); W. Grimus, R. Pfeiffer and T. Schwetz, Eur. Phys. J. C **13**, 125 (2000).

[14] J.J. Gomez-Cadenas and M.C. Gonzalez-Garcia, Z. Phys. **C71**, 443 (1996); N. Okada and O. Yasuda, Int. J. Mod. Phys. **A12**, 3669 (1997); S. Goswami, Phys. Rev. **D55**, 2931 (1997); S. M. Bilenky, C. Giunti, and W. Grimus, Phys. Rev. **D57**, 1920 (1998); S. M. Bilenky, C. Giunti, and W. Grimus, Phys. Rev. **D58**, 033001 (1998); S.M. Bilenky, C. Giunti, W. Grimus and T. Schwetz, Astropart. Phys. **11**, 413 (1999); V. Barger, Y.B. Dai, K. Whisnant and B.L. Young, Phys. Rev. D **59**, 113010 (1999); V. Barger, T.J. Weiler and K. Whisnant, Phys. Lett. B **427**, 97 (1998); C. Giunti, Phys. Rev. D **61**, 036002 (2000); C. Giunti, Phys. Lett. B **467**, 83 (1999); S.M. Bilenky *et al.*,Phys. Lett.

14

B **465**, 193 (1999); C. Giunti, JHEP **0001**, 032 (2000); A. Ibarra and I. Navarro, JHEP **0002**, 031 (2000).

[15] S.M. Bilenky, C. Giunti and W. Grimus, Eur. Phys. J. C **1**, 247 (1998), Proc. of *Neutrino '96*, Helsinki, June 1996, edited by K. Enqvist *et al.*, p. 174, World Scientific, 1997, hep-ph/9609343; S. M. Bilenky, C. Giunti, W. Grimus, and T. Schwetz, Phys. Rev. **D60**, 073007 (1999).

[16] V. Barger, S. Pakvasa, T. J. Weiler, and K. Whisnant, Phys. Rev. **D58**, 093016 (1998).

[17] D. Dooling, C. Giunti, K. Kang and C.W. Kim, Phys. Rev. D **61**, 073011 (2000).

[18] N. Fornengo, M. C. Gonzalez-Garcia and J. W. F. Valle, Nucl. Phys. **B580** (2000) 58; M.C. Gonzalez-Garcia, H. Nunokawa, O.L. Peres and J. W. F. Valle, Nucl. Phys. **B543**, 3 (1999) and M. C. Gonzalez-Garcia.

[19] R. Foot, R.R. Volkas and O. Yasuda, Phys. Rev. **D58**, 013006 (1998); O. Yasuda, Phys. Rev. **D58**, 091301 (1998); E.Kh. Akhmedov, A. Dighe, P. Lipari and A.Yu. Smirnov, Nucl. Phys. **B542**, 3 (1999).

[20] P. Lipari and M. Lusignoli, Phys. Rev. D **58**, 73005 (1998); Q. Y. Liu and A. Yu. Smirnov, Nucl. Phys. B **524**, 505 (1998); Q. Y. Liu, S. P. Mikheyev, and A. Yu. Smirnov, Phys. Lett. B **440**, 319 (1998).

[21] M. C. Gonzalez-Garcia, P. C. de Holanda, C. Peña-Garay and J. W. F. Valle, Nucl. Phys. **B573**, 3 (2000);

[22] J.N. Bahcall, P.I. Krastev, A.Yu. Smirnov, Phys. Rev. **D58**, 096016 (1998).

[23] M. C. Gonzalez-Garcia, C. Peña-Garay, Nucl. Phys. Proc. Suppl. **91**, 80 (2000).

[24] C. Giunti, M. C. Gonzalez-Garcia, C. Peña-Garay, Phys. Rev. **D62**, 013005 (2000); M. C. Gonzalez-Garcia, C. Peña-Garay, Phys. Rev. D **63**, 073013 (2001).

[25] G.L. Fogli, E. Lisi, A. Marrone, Phys. Rev. D **63**, 053008 (2001); hep-ph/0105139.

[26] G.L. Fogli, E. Lisi, A. Marrone, hep-ph/0105139.

[27] O. Yasuda, hep-ph/0006319.

[28] M. Spurio [MACRO Collaboration], hep-ex/0101019; B. Barish [MACRO Collaboration], talk at the XIX International Conference on Neutrino Physics and Astrophysics, Sudbury, Canada, June 2000 (*http://nu2000.sno.laurentian.ca*).

[29] B. Achkar *et al.*, Nucl. Phys. **B424**, 503 (1995).

[30] F. Dydak *et al.*, Phys. Lett. B **134**, 281 (1984).

[31] I. E. Stockdale *et al.*, Phys. Rev. Lett. **52**, 1384 (1984).

[32] V. Barger, B. Kayser, J. Learned, T. Weiler, K. Whisnant, Phys. Lett. **B489**, 345 (2000); O. L. G. Peres , A. Yu. Smirnov, Nucl. Phys. B **599**, 3 (2001); W. Grimus and T. Schwetz, hep-ph/0102252.

[33] C. Giunti and M. Laveder, JHEP **0102**, 001 (2001)

[34] J. N. Bahcall, S. Basu and M. H. Pinsonneault, astro-ph/0010346. See also, http://www.sns.ias.edu/∼bahcall

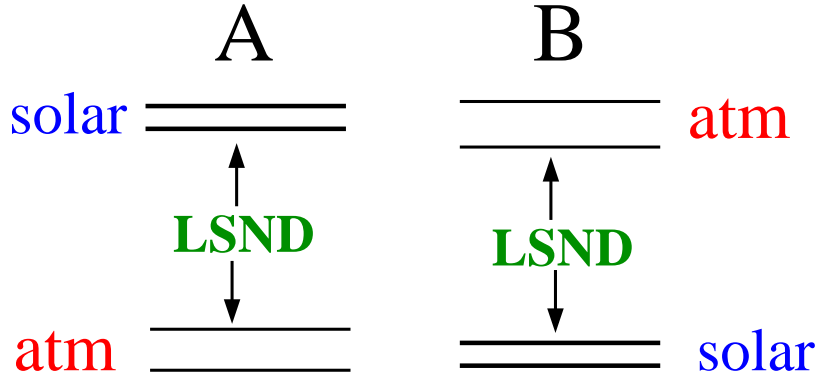[35] M. C. Gonzalez-Garcia, M. Maltoni, C. Pena-Garay and J. W. Valle, Phys. Rev. D **63**, 033005 (2001)

FIG. 1. $2 + 2$ mass schemes in four–neutrino mixing favoured from the combination of solar, atmospheric and LSND results

.

Scenario	$(|U_{\mu 1}|^2 + |U_{\mu 2}|^2 = s_{23}^2)_{\min}$	$(|U_{s1}|^2 + |U_{s2}|^2 = c_{23}^2 c_{24}^2)_{\min}$	$\chi_{\min}^2$	GOF
ATM+SOL$_{\mathrm{unc}}$	0.030	0.91	73.4	65.7%
ATM$_{\mathrm{R}}$+SOL$_{\mathrm{unc}}$	0.	0.97	73.6	68.1%
ATM+SOL$_{\mathrm{LMA}}$	0.065	0.18	76.5	55.9%
ATM$_{\mathrm{R}}$+SOL$_{\mathrm{LMA}}$	0.	0.19	80.1	47.5%
ATM+SOL$_{\mathrm{SMA}}$	0.030	0.91	73.4	65.7%
ATM$_{\mathrm{R}}$+SOL$_{\mathrm{SMA}}$	0.	0.97	73.6	68.1%

TABLE I. $\chi_{\min,\mathrm{atm+sol}}^2$ of the best fit point and its associated GOF in the six–dimensional (five–dimensional for the "restricted" case) space in each of the cases discussed in the text together with the best fit value of the mixings $s_{23}^2 = |U_{\mu 1}|^2 + |U_{\mu 2}|^2$ and $c_{23}^2 c_{24}^2 = |U_{s1}|^2 + |U_{s2}|^2$.
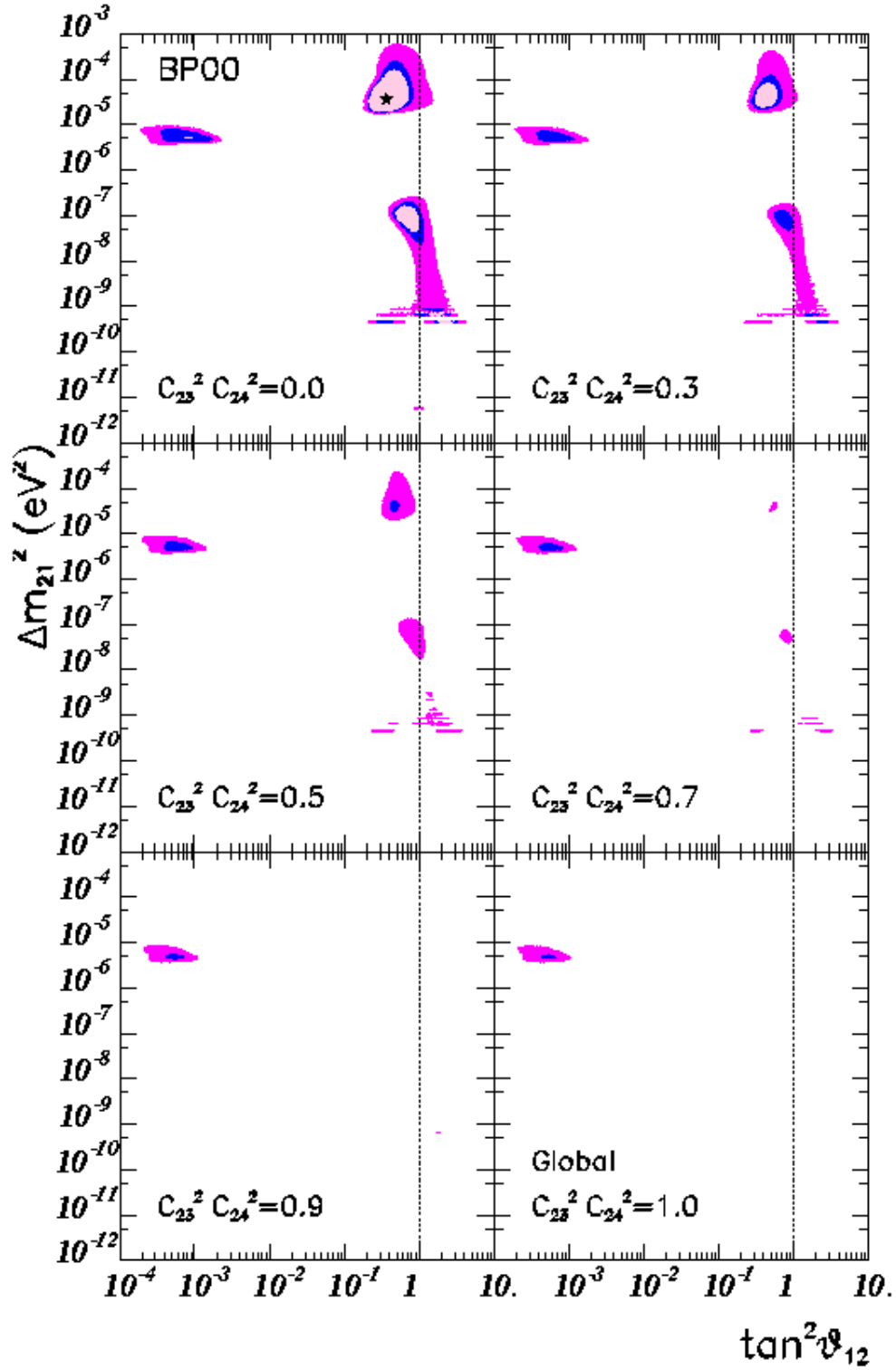
FIG. 2. Results of the global analysis of solar neutrino data for the allowed regions in Δm^2_{21} and $\tan^2 \vartheta_{12}$ for the four–neutrino oscillations. The different panels represent sections at a given value of the active–sterile admixture $|U_{s1}|^2 + |U_{s2}|^2 = c^2_{23} c^2_{24}$ of the three–dimensional allowed regions at 90%, 95% and 99% CL. The best–fit point in the three parameter space is plotted as a star.
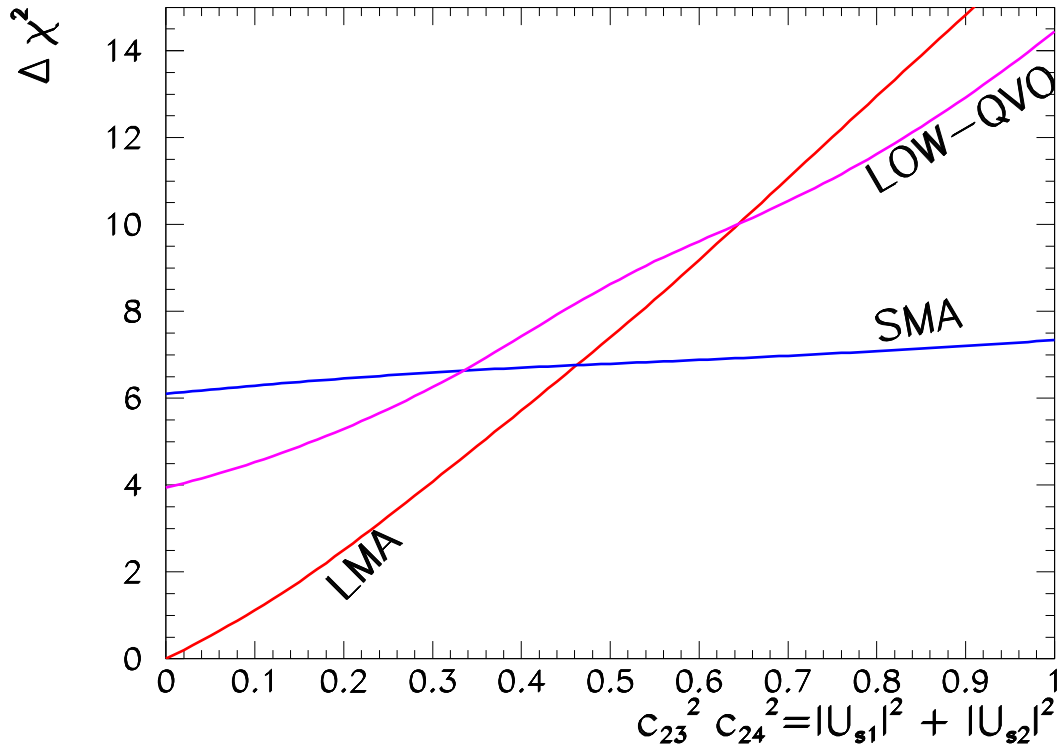
FIG. 3. Difference $\Delta\chi^2$ between the local minimum of χ^2 for each solution of the global analysis of solar neutrino data and the global minimum in the plane $(\tan^2\vartheta_{12}, \Delta m^2_{21})$ as a function of the active–sterile admixture $|U_{s1}|^2 + |U_{s2}|^2 = c^2_{23}c^2_{24}$.
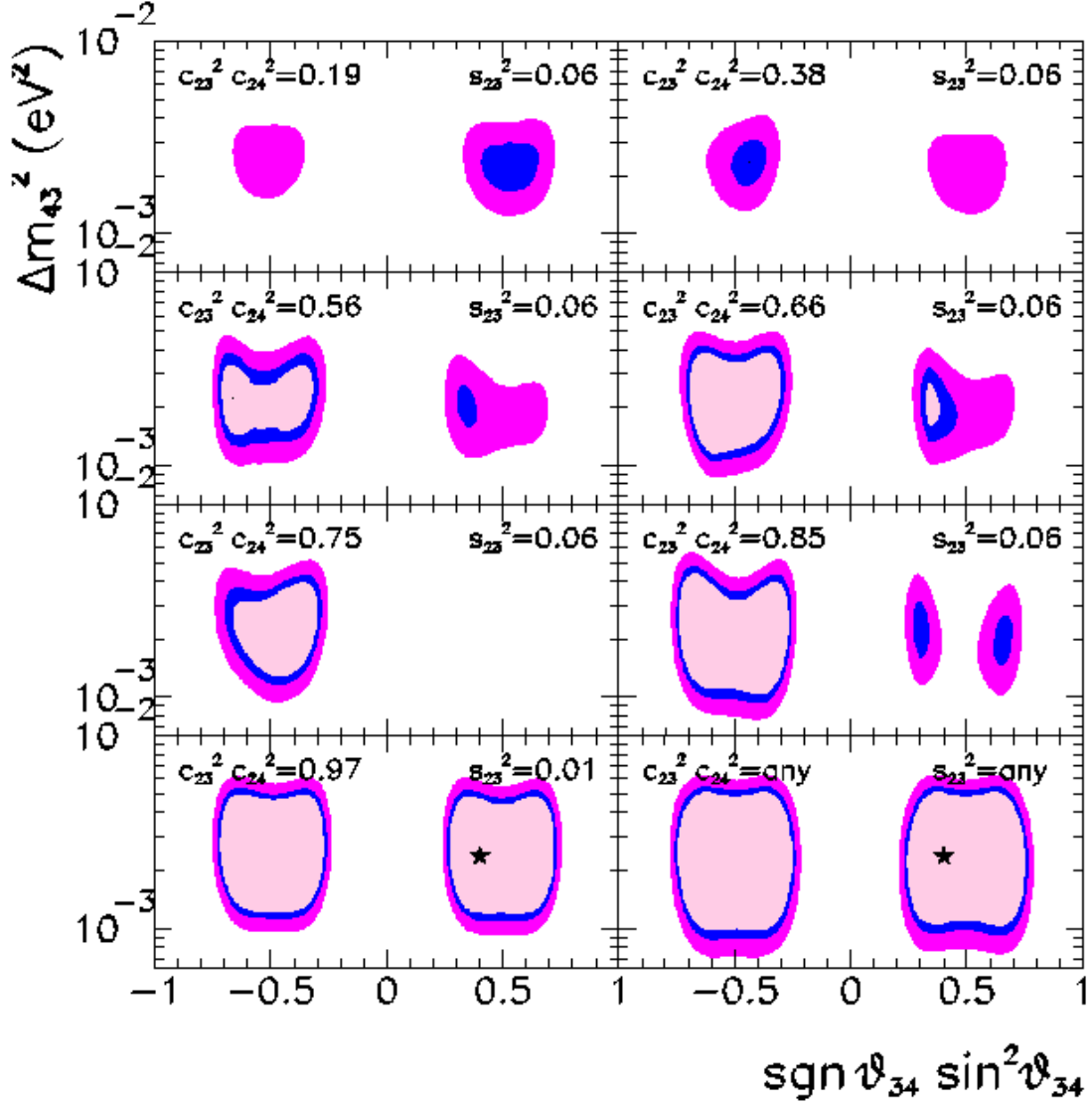
FIG. 4. Results of the analysis of atmospheric neutrino data for the allowed regions in Δm_{43}^2 and ϑ_{34} for the four–neutrino oscillations. The different panels represent sections at given values of the ν_μ projection $|U_{\mu 1}|^2 + |U_{\mu 2}|^2 = s_{23}^2$ and the active–sterile admixture $|U_{s1}|^2 + |U_{s2}|^2 = c_{23}^2 c_{24}^2$ of the four–dimensional allowed regions at 90%, 95% and 99% CL. The best–fit point in the four–parameter space is plotted as a star. The last panel corresponds to the case in which χ^2 has also been minimized with respect to the s_{23}^2 and $c_{23}^2 c_{24}^2$.
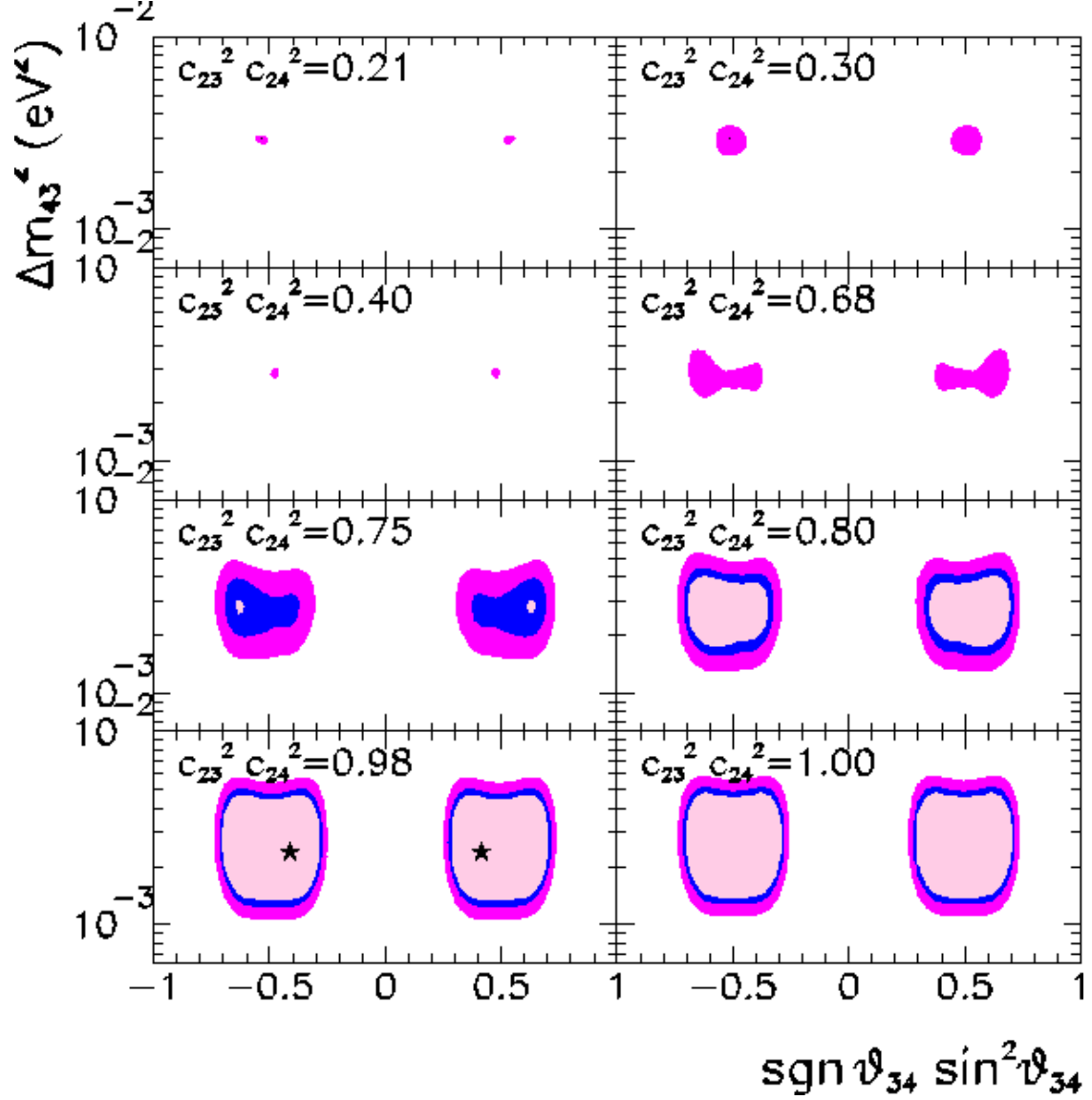
FIG. 5. Results of the analysis of atmospheric neutrino data for the allowed regions in Δm_{43}^2 and ϑ_{34} for the four–neutrino oscillations in the "restricted" case of ν_μ projection $|U_{\mu 1}|^2 + |U_{\mu 2}|^2 = s_{23}^2 = 0$. The different panels represent sections at given values of the active–sterile admixture $|U_{s1}|^2 + |U_{s2}|^2 = c_{24}^2$ of the three–dimensional allowed regions at 90%, 95% and 99% CL. The best–fit point in the three–parameter space is plotted as a star.
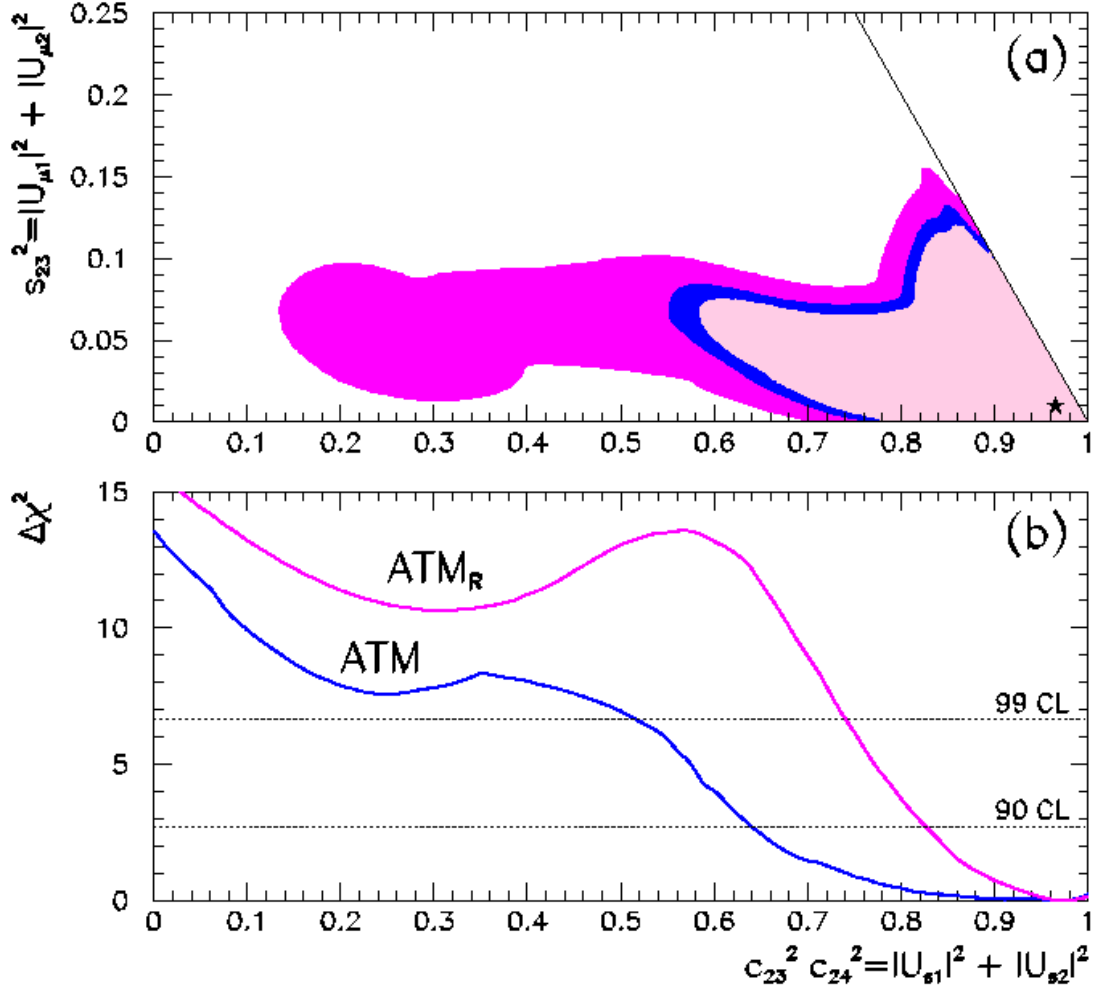
FIG. 6. (a) 90%, 95% and 99% CL allowed regions for the ν_μ projection $|U_{\mu 1}|^2 + |U_{\mu 2}|^2 = s_{23}^2$ and the active–sterile admixture $|U_{s1}|^2 + |U_{s2}|^2 = c_{23}^2 c_{24}^2$ from the analysis of the atmospheric data (see text for details). (b) $\Delta\chi^2$ as a function of the active–sterile admixture $|U_{s1}|^2 + |U_{s2}|^2 = c_{23}^2 c_{24}^2$. In the lower curve χ^2 has been minimized with respect to ϑ_{34}, Δm_{43}^2 and the ν_μ projection $|U_{\mu 1}|^2 + |U_{\mu 2}|^2 = s_{23}^2$. The upper curve corresponds to the "restricted" case $|U_{\mu 1}|^2 + |U_{\mu 2}|^2 = s_{23}^2 = 0$, for which χ^2 has been minimized only with respect to ϑ_{34} and Δm_{43}^2.
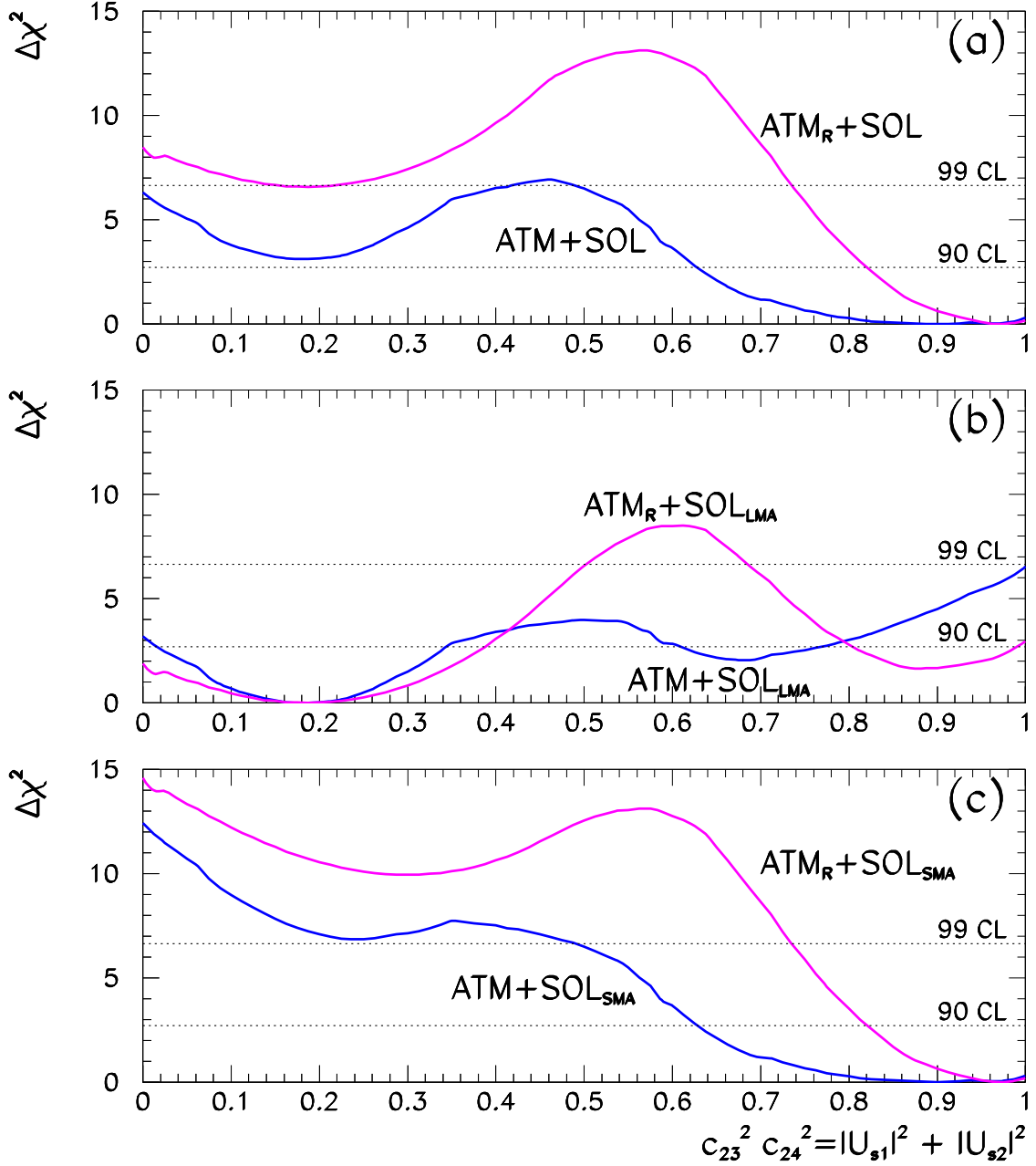
FIG. 7. $\Delta\chi^2$ as a function of the active–sterile admixture $|U_{s1}|^2 + |U_{s2}|^2 = c_{23}^2 c_{24}^2$. In the ATM curves χ^2 have been minimized with respect to ϑ_{34}, Δm_{43}^2 and the ν_μ projection $|U_{\mu1}|^2 + |U_{\mu2}|^2 = s_{23}^2$, as well as with respect to the 1–2 parameters ϑ_{12} and Δm_{21}^2. The ATM$_R$ curves correspond to the "restricted" case $|U_{\mu1}|^2 + |U_{\mu2}|^2 = s_{23}^2 = 0$, so χ^2 has been minimized only with respect to θ_{34}, Δm_{43}^2 and the 1–2 parameters. In (a) the 1–2 parameters ϑ_{12} and Δm_{21}^2 have been minimized in the full parameter space while in (b) [(c)] they have been restricted to lie in the LMA [SMA] solution region.